Finite element analysis of optical bistability in one-dimensional nonlinear photonic band gap structures with a defect

A. Suryanto*, E. van Groesen and. M. Hammer
MESA$^+$ Research Institute, University of Twente, The Netherlands

September 27, 2002

Abstract

We present a new approach based on the recently reported finite element scheme [16] to study the optical response of a finite one-dimensional nonlinear grating. Using the transmitted wave amplitude as a numerical input parameter, we are able to find all stable and unstable solutions related to a specific incident wave which build up the complete bistability curve. The method is applied to investigate the optical bistability in a nonlinear quarter-wave reflector with a defect. With a proper choice of the incident light frequency, a very low bistability threshold is predicted for an optimized defect structure.

1 Introduction

The propagation of waves through periodic dielectric structures, called photonic band gap structures (PBG), has been extensively studied in recent years (see e.g. Ref. [1]-[3]). An essential property of these structures is the existence of a frequency band gap in which light propagation is forbidden. This is analogous to the electronic band gaps in semiconductor crystals. In a crystal, a moving electron experiences a periodic potential produced by the atomic lattice, which produces a gap in the electronic energy band. This gap splits the energy band into two parts: the lower energy band is called the valence band and the high energy band is the conduction band. The optical analogy is the photonic crystal where the periodic potential is due to a lattice of different macroscopic dielectric media.

When Kerr nonlinearity is introduced in the PBG structures (the effective refractive index now depends on the field intensity) it can alter the transmission spectrum including the position of the band-edges. This dynamic shifting of the band-edges can produce optical bistability phenomena (see. e.g. Ref. [4]-[5]), where the threshold value of bistability needed by a PBG is relatively high. Introducing a defect into an otherwise strictly periodic PBG structure can enlarge the nonlinear effect, thus reduce the threshold of bistability. It was shown that the defect creates a donor or acceptor mode in the band gap [6]. Similar to the case of an electron being localized around a defect mode, there is a large field enhancement in the optical defect structure. Since the field intensity inside the defect structure can be very high, the nonlinearity can be enhanced considerably.

Since 30 years ago, a lot of efforts have been devoted to study the phenomenon of bistability in a periodic structure. A number of authors, e.g. Marburger and Felber [7], Winful *et al.* [8], Danckaert *et al.* [9] and [10] proposed an analytical formalism for this problem. All these formalisms are derived within three basic approximations, i.e. the slowly varying envelope approximation (SVEA), the approximation of nonlinear terms that appear in the interface conditions, and the omission of spatial third harmonics

*Applied Mathematics, University of Twente, P.O. Box 217, 7500 AE Enschede, The Netherlands; on leave from Jurusan Matematika, Universitas Brawijaya, Jl. MT Haryono 167 Malang, Indonesia; email:A.Suryanto@math.utwente.nl

generated in the structure. Treatments that make use of the full nonlinear interface conditions in the nonlinear transfer matrix were given by Agarwal and Dutta Gupta [11] and Dutta Gupta and Agarwal [12].

Another approach to solve the nonlinear wave equation was proposed by Chen and Mills [13] and [14]. In this approach the nonlinear Helmholtz equation is transformed into a phase-amplitude equation. By combining with energy conservation the phase-amplitude equation is written in integral form. The integral equation together with the continuity conditions at the interfaces are solved numerically. Recently this method has been implemented by Lidorikis *et al.* [15] to investigate the localized mode solution for a single nonlinear layer sandwiched between two linear periodic structures.

A semi-analytic method has been proposed by Wang *et al.* [5] to study the optical bistability in a linear structure with a single nonlinear defect layer in the center. The transfer matrix method is used for the linear part and a finite difference method is implemented for the nonlinear layer. The left and right linear parts and the nonlinear layer are linked using appropriate interface conditions.

In our earlier work [16] we have developed a robust finite element scheme to study the optical bistability in a one-dimensional (1D) finite grating structure without and with defect. It directly implements the nonlinear Helmholtz equation and exact transparent-influx boundary conditions with the amplitude of the incident wave as the input parameter. The resulting nonlinear system is solved using a weighted-averaged fixed-point iterative method. This approach can capture the bistability phenomena where the method can only find the two stable solutions but not the unstable solutions. In case of multistability, it will be very difficult to find more than two stable solutions. In addition, the convergence of the iteration procedure can be very slow in the region of upswitching from low-output level to high-output level.

For a fixed frequency light propagation through the multilayer structures that are discussed here, optical bistability manifests itself by a non-unique dependence of the transmission on the power of the incident wave. Contrarily, when viewing the input power as a function of the transmission, the dependence was observed to be unique (see e.g. Ref. [16]). Therefore in this paper we refine the performance of our scheme by using the transmitted wave as the input parameter instead of the incident wave. This method will be discussed in Sec. 2. Here we focus only on a 1D PBG structure where a defect has been introduced. In Sec. 3 we apply our numerical scheme to study the optical response of a defect structure. We first focus on the linear structure and study the influence of the defect thickness, the position and the refractive index of the defect layer, and the number of layer periods. Subsequently, we consider effect of the nonlinearity. Conclusions and remarks will be given in the last section.

2 1D PBG Structure and Numerical Method

Consider a one-dimensional finite quarter-wavelength stack which is composed of alternating layers of dispersionless and lossless materials which have a high refractive index n_H (denoted as H layer) and a low refractive index n_L (denoted as L layer). Fig. 1 illustrates the geometry. The thicknesses for the two kinds of layers are such that $d_L = \lambda_0/4n_L$ and $d_H = \lambda_0/4n_H$, where λ_0 is the free-space design wavelength. We assume that the front and back media have refractive index n_0. It is also assumed that the high-index layer shows a positive Kerr nonlinearity. The defect structure can be obtained by simply perturbing the thickness of any layer (which is then called a defect layer and is denoted by D) or by changing the refractive index of the defect layer. For simplicity we denote the defect structure as $(HL)^{N_1}(D)^M(LH)^{N_2}$, where N_1 and N_2 are respectively the number of layer periods in the left and right of the defect layer and M is the multiple of the defect layer with a unit thickness of $\lambda_0/4n_d$. This means that the thickness of the defect layer is $L_d = M \times (\lambda_0/4n_d)$, with n_d being the refractive index of the defect layer.

The electric field amplitude of the normally incident, monochromatic wave with frequency ω and vacuum wave number $k = \omega/c$ is modelled by the nonlinear Helmholtz equation (NLH)

$$\frac{d^2E}{dz^2} + k^2\left(n^2(z) + \chi^{(3)}(z)\,|E|^2\right)E(z) = 0, \tag{1}$$

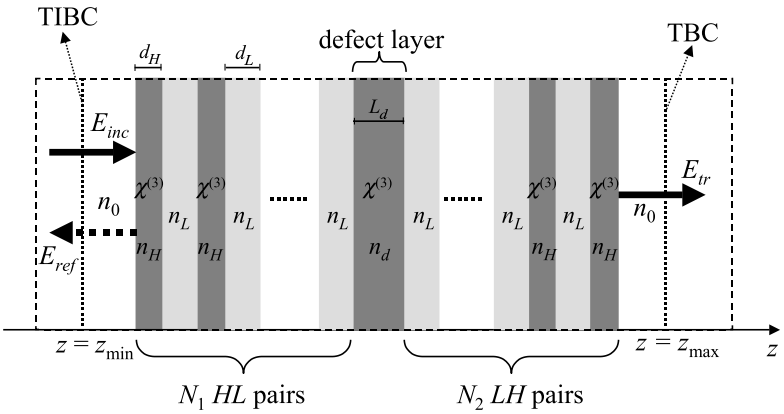

Figure 1: Schematic view of the 1D PBG structures considered in this paper which are composed of N_1 HL layers and N_2 LH layers separated by a defect layer with thickness $L_d = M \times (\lambda_0/4n_d)$. The thicknesses of layers H and L are respectively $d_H = \lambda_0/4n_H$ and $d_L = \lambda_0/4n_L$. The medium outside the structure is linear homogeneous with refractive index n_0. For the numerical calculations we introduce a transparent-influx boundary condition (TIBC) and transparent boundary condition (TBC) in the left and right hand side of the structure.

where $c = 1/\sqrt{\varepsilon_0 \mu_0}$ is the speed of light in vacuum and $\chi^{(3)}$ is the third order nonlinearity, see e.g Ref. [16]. Since the front and back media of our structure have a uniform index n_0, the two boundary conditions for the NLH (1) are given by

$$\frac{dE}{dz} - ikn_0 E = -2ikn_0 A_{inc}, \quad z = z_{\min} \tag{2}$$

$$\frac{dE}{dz} + ikn_0 E = 0, \qquad z = z_{\max}. \tag{3}$$

The first boundary condition (2) is an influx condition for an incident wave with wavenumber k and constant real amplitude A_{inc}. It is also simultaneously transparent for the reflected wave (therefore it is called transparent-influx boundary condition (TIBC)). The second condition (3) is a transparent boundary condition (TBC) for the right-travelling wave, see Ref. [16].

In our previous work [16] we have developed a finite element scheme to solve the NLH (1) together with the boundary conditions (2) and (3). We start by writing the functional of the problem:

$$\mathcal{F}(E) = -\frac{1}{2}\int_{-\infty}^{\infty} \left(\left| \frac{dE}{dz} \right|^2 - k^2 n^2 |E|^2 - \frac{1}{2} k^2 \chi^{(3)} |E|^4 \right) dz \tag{4}$$

which can also be written as

$$\mathcal{F}(E) = \mathcal{F}_1(E) + \mathcal{F}_2(E) + \mathcal{F}_3(E) \tag{5}$$

where

$$\mathcal{F}_1(E) = -\frac{1}{2}\int_{-\infty}^{z_{\min}} \left(\left| \frac{dE}{dz} \right|^2 - k^2 n_0^2 |E|^2 \right) dz,$$

$$\mathcal{F}_2(E) = -\frac{1}{2}\int_{z_{\min}}^{z_{\max}} \left(\left| \frac{dE}{dz} \right|^2 - k^2 n^2 |E|^2 - \frac{1}{2} k^2 \chi^{(3)} |E|^4 \right) dz,$$

$$\mathcal{F}_3(E) = -\frac{1}{2}\int_{z_{\max}}^{\infty} \left(\left| \frac{dE}{dz} \right|^2 - k^2 n_0^2 |E|^2 \right) dz.$$

As it is assumed that the medium outside the grating structure is linear homogeneous with refractive index n_0, without loss of generality, the solution of equation (1) can be written as

$$E(z) = \begin{cases} A_{inc} \exp\left(-ikn_0 \left(z - z_{\min}\right)\right) + A_{ref} \exp\left(ikn_0 \left(z - z_{\min}\right)\right) & , \quad z \leq z_{\min}; \\ E(z) & , \ z \in [z_{\min}, z_{\max}]; \\ A_{tr} \exp\left(-ikn_0 \left(z - z_{\max}\right)\right) & , \quad z \geq z_{\max}; \end{cases} \tag{6}$$

where A_{inc} and A_{ref} are respectively the amplitudes of the incident and the reflected waves and A_{tr} is the transmitted wave amplitude. By substituting (6) into the functional (5), one can show that if the variational derivative of this functional vanishes, $\delta_E \mathcal{F} = 0$, then the field $E(z)$ satisfies the NLH (1) and its boundary conditions (2) and (3).

In the derivation of the numerical scheme, we approximate the functional $\mathcal{F}_2(z)$ by writing the function $E(z)$ as a linear combination of a standard linear basis $\{\varphi_m(z)\}_0^{M_0}$:

$$E(z) \cong \sum_{j=0}^{M_0} \widehat{E}_j \varphi_j(z) \tag{7}$$

such that

$$\mathcal{F}_2(E) \cong \widetilde{\mathcal{F}}_2\left(\widehat{E}\right) \tag{8}$$

where $\widehat{E} = \begin{pmatrix} \widehat{E}_0, & \widehat{E}_1, & \cdots, & \widehat{E}_{M_0} \end{pmatrix}^T$. Here we assume that the interval $[z_{\min}, z_{\max}]$ is divided into M_0 subintervals of equal length $h = (z_{\max} - z_{\min})/M_0$ by choosing the nodal points $z_j = z_{\min} + jh$ for $j = 0, 1, \ldots, M_0$. $\widehat{E}_j$ is the approximation of $E(z)$ at $z = z_j$. The condition $\delta_E \mathcal{F} = 0$ therefore corresponds to $\delta_E \mathcal{F}_1 + \nabla \widetilde{\mathcal{F}}_2\left(\widehat{E}\right) + \delta_E \mathcal{F}_3 = 0$ which leads to the finite element scheme

$$\left(\frac{1}{h}P + \frac{1}{6}hk^2 Q + R\left(\widehat{E}\right)\right)\widehat{E} = v, \tag{9}$$

where

$$P = \begin{pmatrix} -1 - ihkn_0 & 1 & 0 & . & . & 0 \\ 1 & -2 & 1 & 0 & . & . \\ 0 & . & . & . & . & 0 \\ . & . & 0 & 1 & -2 & 1 \\ 0 & . & . & 0 & 1 & -1 - ihkn_0 \end{pmatrix},$$

$$Q = \begin{pmatrix} 2\widehat{n}_0^2 & \widehat{n}_0^2 & 0 & . & . & 0 \\ \widehat{n}_0^2 & 2\left(\widehat{n}_0^2 + \widehat{n}_1^2\right) & \widehat{n}_1^2 & 0 & . & . \\ 0 & . & . & . & . & 0 \\ . & . & 0 & \widehat{n}_{M_0-2}^2 & 2\left(\widehat{n}_{M_0-2}^2 + \widehat{n}_{M_0-1}^2\right) & \widehat{n}_{M_0-1}^2 \\ 0 & . & . & 0 & \widehat{n}_{M_0-1}^2 & 2\widehat{n}_{M_0-1}^2 \end{pmatrix},$$

$\widetilde{\nabla F_{NL}}\left(\widehat{E}\right) = R\left(\widehat{E}\right) \cdot \widehat{E}$ and $v = \begin{pmatrix} -2ikn_0 A_{inc} & 0 & \ldots & 0 \end{pmatrix}^T$ with

$$\begin{aligned} \frac{\partial \widetilde{F_{NL}}}{\partial \widehat{E}_j} &= \mu_{j-1}\left(\frac{2}{3}\widehat{E}_{j-1}\widehat{E}_j^* + \left|\widehat{E}_{j-1}\right|^2 + 2\left|\widehat{E}_j\right|^2\right)\widehat{E}_{j-1} \\ &+ \mu_{j-1}\left(\widehat{E}_j\widehat{E}_{j-1}^* + \frac{4}{3}\left|\widehat{E}_{j-1}\right|^2 + 4\left|\widehat{E}_j\right|^2\right)\widehat{E}_j \\ &+ \mu_j\left(\widehat{E}_j\widehat{E}_{j+1}^* + \frac{4}{3}\left|\widehat{E}_{j+1}\right|^2 + 4\left|\widehat{E}_j\right|^2\right)\widehat{E}_j \\ &+ \mu_j\left(\frac{2}{3}\widehat{E}_{j+1}\widehat{E}_j^* + \left|\widehat{E}_{j+1}\right|^2 + 2\left|\widehat{E}_j\right|^2\right)\widehat{E}_{j+1}, \end{aligned}$$

and $\mu_j = hk^2\chi_j^{(3)}/20$. Here $\widehat{n}_j$ and $\chi_j^{(3)}$ are the linear refractive index and the strength of the nonlinearity in the interval (z_j, z_{j+1}), respectively. One can check that the scheme (9) is second-order accurate. However, as shown in [16], the linear part of this scheme can be improved to get a fourth-order scheme

$$\left(\frac{1}{h}P_1 + \frac{1}{6}hk^2Q + R\left(\widehat{E}\right)\right)\widehat{E} = v_1, \tag{10}$$

i.e., by replacing P and v in (9) with P_1 and v_1, respectively where

$$P_1 = \begin{pmatrix} -\alpha_0\left(1+ihkn_0\right) & \alpha_0 & 0 & . & . & 0 \\ \alpha_0 & -\left(\alpha_0+\alpha_1\right) & \alpha_1 & 0 & . & . \\ 0 & . & . & . & . & 0 \\ . & . & 0 & \alpha_{M_0-2} & -\left(\alpha_{M_0-2}+\alpha_{M_0-1}\right) & \alpha_{M_0-1} \\ 0 & . & . & 0 & \alpha_{M_0-1} & -\alpha_{M_0-1}\left(1+ihkn_0\right) \end{pmatrix},$$

with $\alpha_j = 1 - \frac{1}{12}k^2\widehat{n}_j^2h^2$ and $v_1 = \begin{pmatrix} -2ikA_{inc}\left(1+k^2n_0^2h^2/12\right) & 0 & \cdots & 0 \end{pmatrix}^T$. The system of nonlinear equations (10) can be solved using a weighted-averaged fixed-point iterative method combined with a continuation method. Using the incident wave amplitude A_{inc} as an input parameter (fixed input problem), we have shown in Ref. [16] that this iterative procedure is able to find the two stable solutions in a bistable configuration, but it does not give access to unstable solutions. Unfortunately, when the nonlinear effect is relatively high the convergence of this method can be very slow, especially in the interval near the jumping area from the low-output state into the high-output state. Furthermore, in the case of multistability, it will be very difficult to find more than two stable solutions.

In this paper we improve the performance of our finite element scheme. Instead of the incident wave, we use the transmitted wave as the input parameter. This approach is called a fixed output problem. As stated in (6), the transmitted wave in the homogeneous medium beyond the defect structure is of the form

$$E(z) = A_{tr}\exp\left(-ikn_0\left(z - z_{\max}\right)\right), \qquad z \geq z_{\max}. \tag{11}$$

Without loss of generality, we assume that the transmitted wave amplitude A_{tr} is a real constant. Consequently the value of the incident wave amplitude A_{inc} now can be a complex number. In this approach the nonlinear system (10) is reformulated such that A_{inc} is included as an unknown variable and A_{tr} is the input parameter:

$$\begin{pmatrix} \begin{pmatrix} 2ik\left(1+k^2n_0^2h^2/12\right) \\ 0 \\ \vdots \\ 0 \\ (0) \end{pmatrix} & \begin{matrix} \left(\frac{1}{h}P_1 + \frac{1}{6}hk^2Q + R\left(\widehat{E}\right)\right) \\ \\ \begin{pmatrix} 0 & \cdots & 0 & 1 \end{pmatrix} \end{matrix} \end{pmatrix} \begin{pmatrix} A_{inc} \\ \widehat{E}_0 \\ \widehat{E}_1 \\ \vdots \\ \widehat{E}_{M_0-1} \\ \widehat{E}_{M_0} \end{pmatrix} = \begin{pmatrix} 0 \\ \vdots \\ 0 \\ A_{tr} \end{pmatrix}. \tag{12}$$

We solve the nonlinear system (12) using a standard fixed-point iterative method. As shown in the next section this method can find all stable and unstable solutions related to a specific incident wave which build up the full bistability (or multistability) curve. We also notice that the convergence of this approach is much faster than that of the fixed input problem.

3 Optical Bistability in a 1D PBG Structure with a Defect

In this section we apply the numerical scheme that was derived in the previous section to study the optical response of linear and nonlinear defect structures. For the numerical calculations we take $n_L = 1.25$ and $n_H = 2.5$. Unless it is mentioned otherwise, the refractive index of the input and output regions $z < 0$ and $z > z_{\max}$ is assumed to be $n_0 = 1$ and that of the defect layer is $n_d = n_H$. The computational window is divided into M_0 equidistant elements with grid size $h = \lambda_0/400$. To get a better understanding of the defect structure, we will discuss first the properties of the linear structure by setting $\chi^{(3)} = 0$.

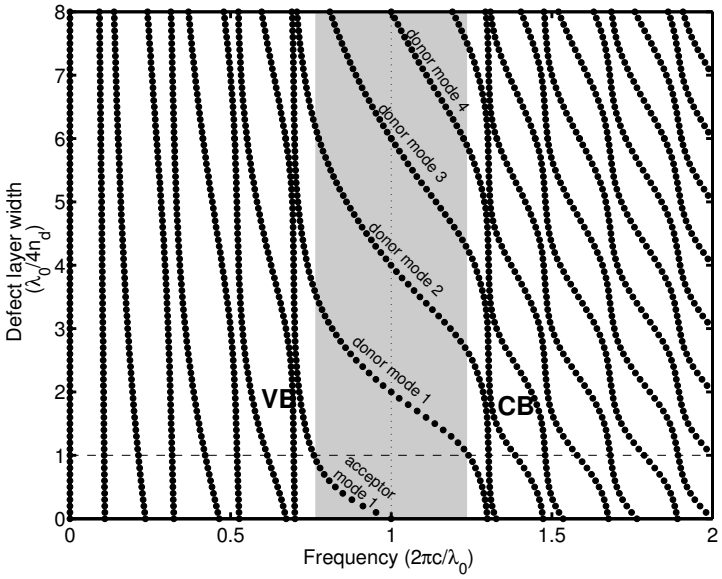

Figure 2: The (frequency) position of transmission maxima as a function of the defect layer width for structure $(HL)^4\,(D)^M\,(LH)^4$ with $n_d = n_H$. The media in the input and output regions are assumed to be air ($n = 1$). The shaded-area indicates the first band gap of the perfect structure, i.e. when the defect layer is $\lambda_0/4n_d$ (see the dashed-line). Observe the appearance of acceptor/donor modes caused by changing the defect size. It is noticed that when two transmission maxima outside the band gap meet, they show an anticrossing behavior.

3.1 Transmission properties of the linear structure

As mentioned in the first section the perfect (infinite) PBG structure has an essential property, i.e. the existence of forbidden bands prohibiting a certain range of frequencies of light waves to propagate through them. In other words, the light waves with frequencies inside the band gap are completely reflected by the structure. However, in a finite periodic structure, the reflection will not be complete in general. Therefore we practically use the term band gap (of a finite structure) for the smallest frequency interval containing the band gap of the infinite structure that is bordered by two resonance frequencies. When a defect is introduced in the structure, it can create a donor or acceptor mode inside the band gap [6] which is similar to the case of a semiconductor. In this section we discuss the dependence of the defect modes on the thickness, the position and the refractive index of the defect layer and the number of layer periods.

Let us start by considering an ideal PBG structure with 17 alternating layers (9 H layers and 8 L layers; the structure has the form $HL...LHL...LH$). Then by disturbing the width of the center layer, which has a high refractive index n_H, we obtain a symmetric defect structure $(HL)^4(D)^M(LH)^4$. In Fig.2 we show the position of transmission maxima where the transmission coefficient is unity as a function of the defect layer width for our defect structure. The perfect structure, i.e. when the thickness of the center layer is $\lambda_0/4n_H$ (see dashed line in Fig. 2) has a band gap which is centered at the frequency $2\pi c/\lambda_0$. The shaded-region indicates the width of the first band gap. This band gap is bordered by two transmission maxima which are often called band-edge modes. The band-edge modes in this case are respectively at $\omega = 0.75915 \times 2\pi c/\lambda_0$ and $\omega = 1.24085 \times 2\pi c/\lambda_0$. By analogy to the solid state electronics case, the frequency band which lies below the band gap is called the valence band (VB) and the upper one is the conduction band (CB). For the ideal structure, as shown in Fig. 2, there are nine transmission maxima inside the VB which correspond to optical Bloch waves that can propagate through the structure. When reducing the defect width, the valence band edge moves into the band gap to become a defect mode.

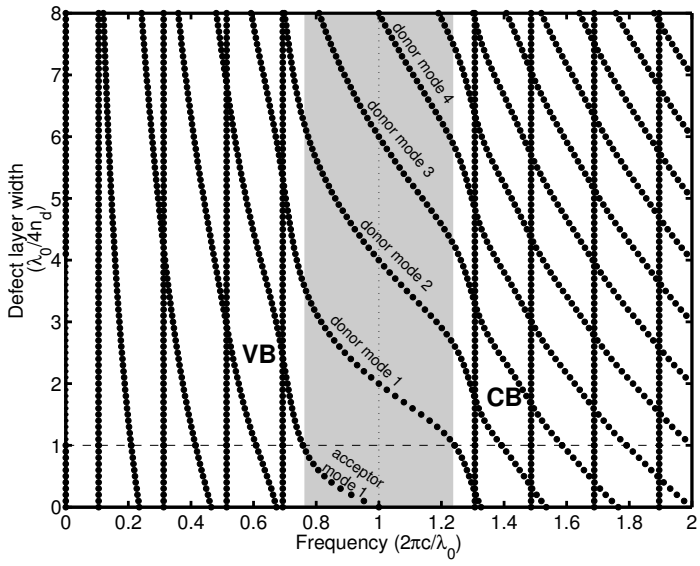

Figure 3: The same as Fig. 2 except that the first and last semi-infinite layers are now assumed to have refractive index $n_0 = n_L$ instead of $n_0 = 1$. Similar to that presented in Fig. 2, acceptor/donor modes are created as we change the thickness of the defect layer. With disturbing the defect layer, two transmission maxima can merge and split but the frequency of one of these two maxima remain the same.

Since the defect mode evolves from the valence band with decreasing the defect size, it can be thought of as an acceptor mode (see e.g. Ref. [6]). We note that the acceptor mode frequency increases as the defect size is decreased. On the other hand, if the width of the center layer of our perfect structure is increased the conduction band edge moves into the band gap region. This type of defect mode is called a donor mode. When the width of the defect layer is further increased more than one defect mode can be obtained. Stanley *et al.* [17] have noticed that the moving behavior of the transmission maxima of the defect structure is identical to the case of solid-states electronic, except for the anticrossing behavior outside the band gap. However, when we assume that the front and the back media have a refractive index n_L instead of air, the anticrossing behavior cannot be observed anymore (see Fig. 3). In this case, as we change the defect layer, two transmission maxima outside the band gap merge and then split again with the frequency of one of these maxima remaining constant.

It is well known that the defect mode can enhance the field intensity inside the structure. By assuming that the incident wave amplitude equals to one, we show in Fig. 4 the enhancement of the field amplitude as a function of the size of the defect layer for donor mode 1, donor mode 2 and donor mode 3, respectively. The field amplitude enhancement here is defined as the maximum field amplitude ($\max|E|$) inside the structure. It is shown in Fig. 4 that for each donor mode the largest enhancement occurs when the width of the defect layer equals to $\alpha\,(\lambda_0/2n_H)$ for integer α. It can be checked in Fig. 2 that those donor modes have the same frequency $\omega = 2\pi c/\lambda_0$. The maximum enhancement of the field amplitude in this case is sixteen times of the incident wave. Although the enhancement factors of structures with defect thicknesses $\alpha\,(\lambda_0/2n_H)$ are the same, the field amplitudes inside the structures are different for different α. By increasing the value of α by one an additional field amplitude peak is observed in the structure, see Fig. 5. Moreover, the change of α will also change the spectral width of the defect mode. It is clearly seen in Fig. 6 that the full width at half maximum (FWHM) of the defect mode decreases with increasing α.

Now we study the influence of the defect position in the structure on the defect mode. We are still considering a structure of 17 alternating layers including 9 H layers and 8 L layers. The defect layer is introduced by changing the size of one of the layer H to be $\lambda_0/2n_H$. The effect of defect position is

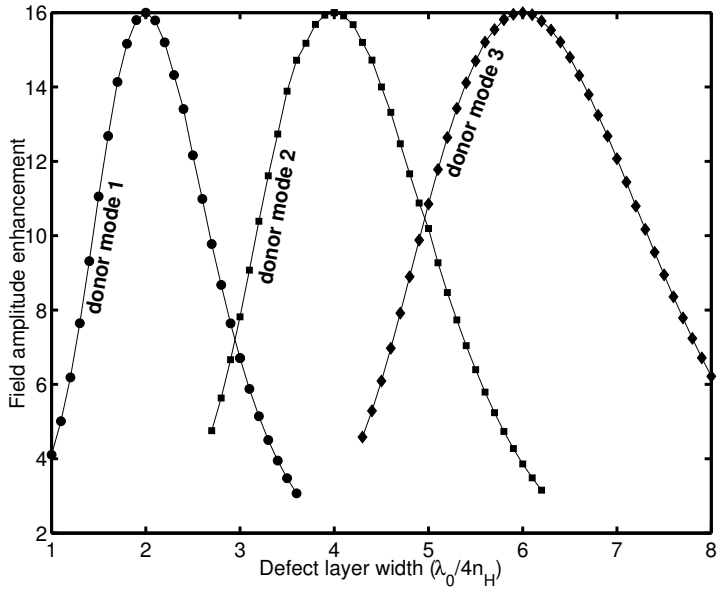

Figure 4: The maximum field enhancement as function of the defect layer width for donor mode 1, 2 and 3. The enhancement factors for those three donor modes are 16 which occur when the defect modes are at $\omega = 2\pi c/\lambda_0$ and the thickness of the defect layer equals to $\alpha\,(\lambda_0/2n_H)$ for integer α.

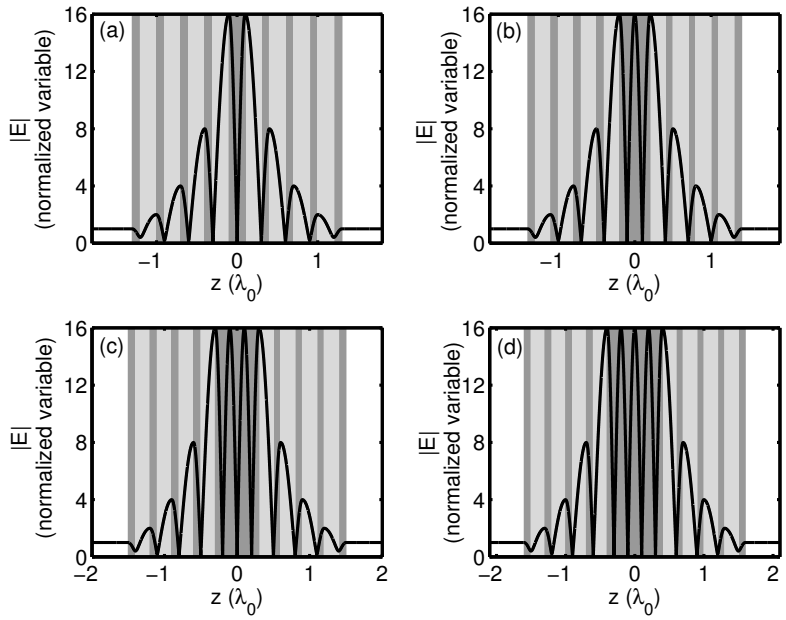

Figure 5: The field amplitude $|E|$ inside the defect structure $(HL)^4\,(D)^M\,(LH)^4$ with $n_d = n_H$ for (a) $L_d = \lambda_0/2n_H$; (b) $L_d = \lambda_0/n_H$; (c) $L_d = 3\lambda_0/2n_H$ and (d) $L_d = 2\lambda_0/n_H$ at frequency $\omega = 2\pi c/\lambda_0$. Observe that the maximum of the amplitude is 16 for all cases. The longer the defect layer is the more amplitude maxima can be observed inside the defect region.

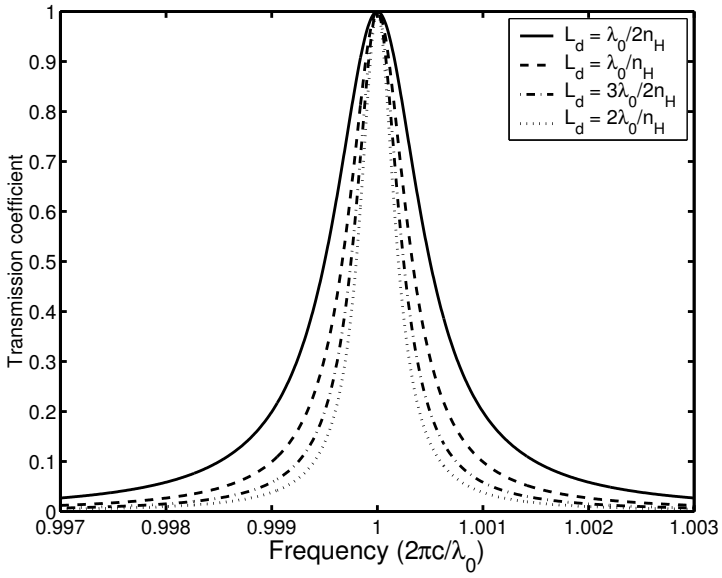

Figure 6: The transmission spectrum around the defect mode for different defect layer widths. The spectral width of the defect mode decreases with the increasing defect L_d.

investigated by moving the defect layer from the left to the right of the structure. It is found that the changing of the defect position disturbs the positions of the transmission maxima outside the band gap. However the position of the defect mode remains the same, i.e. at frequency $2\pi c/\lambda_0$. Furthermore, the transmission coefficients of those transmission maxima including the defect mode can be less than one when the defect layer is not located at the center of the structure. Because we are more interested in the defect mode, we plot in Fig. 7 the transmission coefficient of the defect mode as a function of the position of the defect layer. The incident wave is fully transmitted by the defect structure only when the defect layer is placed in the center of the structure. Otherwise the incident light is partly reflected. Wang *et al.* [18] explain this phenomena by considering the whole defect structure as two smaller structures linked together, i.e. one is structure with a defect in the middle and the other is a perfect structure. Incident light with frequency of the defect mode can pass through the defect part, but is partly reflected by the perfect part because its frequency is in its band gap. Therefore, the structure with a central defect layer has the highest transmission coefficient.

Next we investigate the dependence of the defect mode on the refractive index of the defect layer. The defect structure considered here has the form $(HL)^4 (D)^M (LH)^4$. The index of the defect layer n_d is varied from 2 to 4. According to the results of our calculations, an acceptor mode appears in the band gap if the defect thickness is less than $\lambda_0/4n_d$. On the contrary, some donor modes can be obtained if the size of the defect layer is greater than $\lambda_0/4n_d$. Similar to the previous case the enhancement factor of the field amplitude is sixteen and is obtained when the width of the defect layer is a multiple of $\lambda_0/2n_d$ (i.e. when M is an even number) at defect mode frequency $2\pi c/\lambda_0$. Furthermore the FWHM of the defect mode of a structure $(HL)^4 (D)^2 (LH)^4$ becomes smaller as we increase the refractive index of the defect layer, see Fig. 8.

Finally we investigate the effect of the number of layer periods by considering the symmetrical structure $(HL)^N (D)^2 (LH)^N$ for $N = 4, 5, 6, 7$. The index and the width of the defect layer are chosen to be n_H and $\lambda_0/4n_H$, respectively. Using this structure, a defect mode in the center of the band gap of the corresponding perfect structure can be found. Fig. 9 shows the field amplitude inside the structure for different N. The maximum field intensity is changed as the number of periods changes. A larger N produces a larger field amplitude enhancement. More precisely the enhancement factors of structures with $N = 4, 5, 6, 7$ are respectively $16, 32, 64$ and 128 which are exactly 2^N. In addition to the increasing

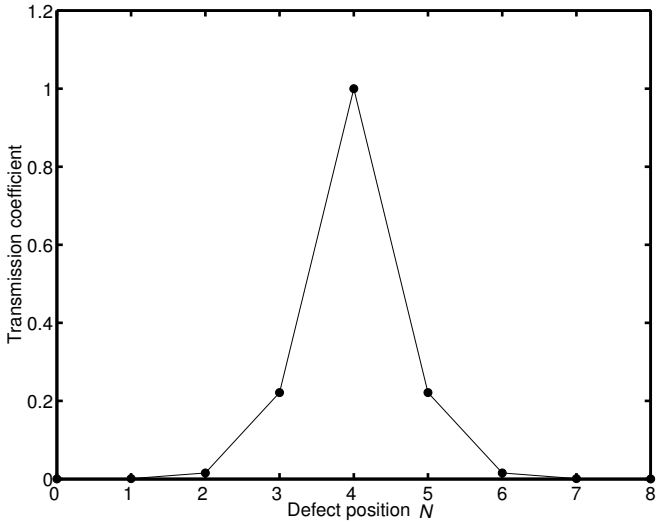

Figure 7: The transmission coefficient at $\omega = 2\pi c/\lambda_0$ of a defect structure $(HL)^N (D)^2 (LH)^{8-N}$ for $N = 0, 1, ..., 8$. The maximum transmission occurs when the defect layer is placed in the middle of the structure.

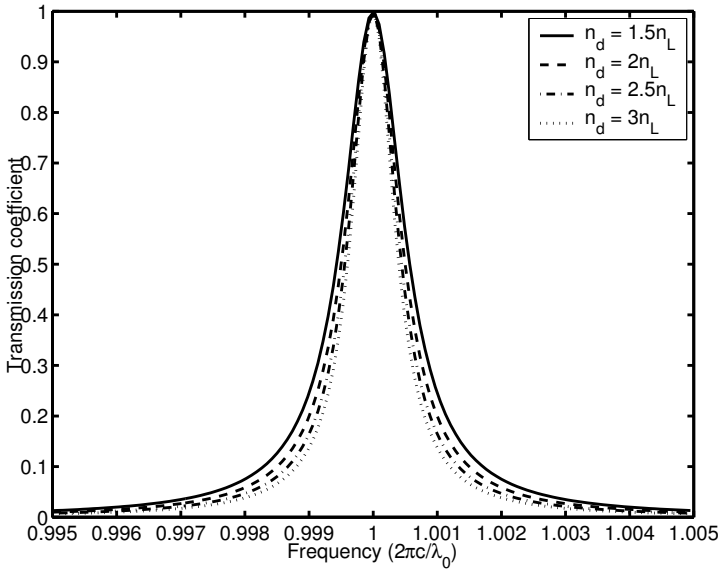

Figure 8: The transmission spectrum around the defect mode of a structure $(HL)^4 (D)^2 (LH)^4$ for different refractive indices of the defect layer. The spectral width of the defect mode decreases when the refractive index of the defect layer is increased.

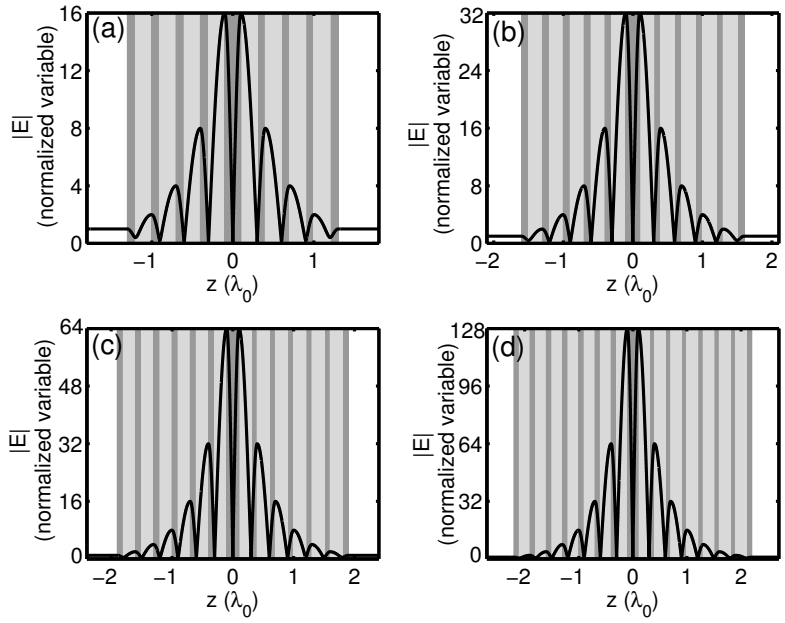

Figure 9: The field amplitude $|E|$ inside the defect structure $(HL)^N (D)^2 (LH)^N$ with $n_d = n_H$ and $L_d = 2(\lambda_0/4n_H)$ for (a) $N = 4$; (b) $N = 5$; (c) $N = 6$ and (d) $N = 7$ at frequency $\omega = 2\pi c/\lambda_0$. The maximum amplitudes for those cases are 2^N.

field enhancement of the defect mode with respect to the increasing N, its spectral width also decreases, see Fig. 10.

It is well known that the enhancement factor and the decrease of the spectral width are important properties for optical bistability. Based on the previous discussion we conclude that to get a high field enhancement a defect structure $(HL)^{N_1} (D)^M (LH)^{N_2}$ is to be designed such that the defect layer is positioned in the middle of the structure, i.e $N_1 = N_2$ with M being an even integer number. Then the defect mode is located in the center of the band gap. A higher value of M leads to a smaller FWHM. Increasing the number of grating periods N yields simultaneously a narrower resonance and a field enhancement that grows exponentially with N.

3.2 Bistable switching controlled by input intensity

If a Kerr nonlinearity is introduced in the structure, it causes a change of local refractive index. According to Ref. [19] the induced refractive index change is proportional to the intensity of the optical field and can be written as

$$\Delta n = \overline{n}_2 |E|^2 \tag{13}$$

where the nonlinear refractive index coefficient $\overline{n}_2$ of the medium is defined by

$$\overline{n}_2 = \frac{1}{2n}\chi^{(3)}. \tag{14}$$

Due to a change of the effective refractive index, the transmission spectrum will also change accordingly. It was shown in Ref. [16] that when a positive Kerr nonlinearity is introduced in all high index layers of a defect structure, the entire transmission spectrum will be shifted dynamically to the left. Specifically when the resonance is sharp enough, e.g. in case of a defect mode, the transmission spectrum can exhibit a bistability phenomenon. Hence, to obtain a bistability behavior the frequency of the input light has

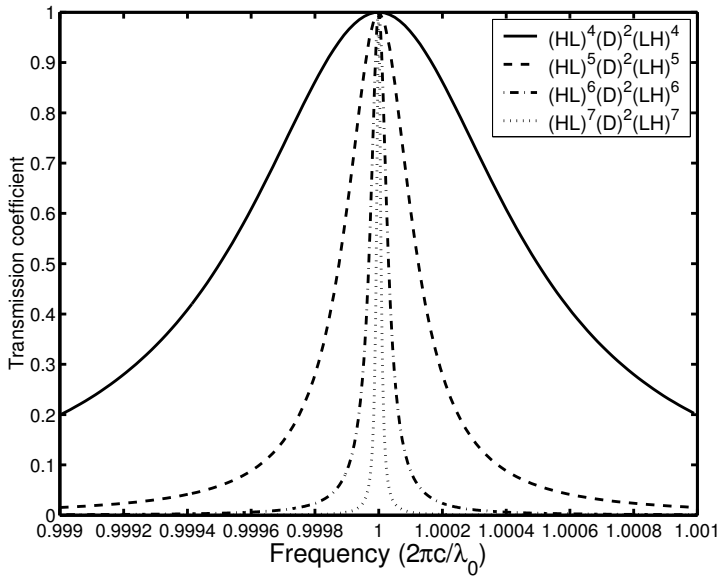

Figure 10: The transmission spectrum around the defect mode of the structures $(HL)^N (D)^2 (LH)^N$ for $N = 4, 5, 6, 7$. The spectral width of the defect mode decreases with growing number of periods N.

to be selected in the vicinity of the defect mode frequency. More precisely, it should be below the defect mode.

A basic issue of the optical bistability is to realize it with threshold as low as possible. A low threshold requires a large nonlinear effect. There are two ways to increase the nonlinear effect, i.e. by using a medium with a high Kerr constant or by designing a structure that can enhance the input intensity. Given the presently available materials with limited Kerr nonlinearity, we, therefore, consider a symmetric defect structure. We assume that a Kerr nonlinearity with $\chi^{(3)} = 2 \times 10^{-12}$ m^{2}V^{-2} is present in all high index layers H as well as in the defect layer.

In Fig. 11 we present the input-output characteristics of the structure $(HL)^4 (D)^2 (LH)^4$ for some frequencies below the defect mode $\omega = 2\pi c/\lambda_0$. It is found that for $\omega = 0.995 \times 2\pi c/\lambda_0$ the structure shows an S-shape response. When the incident intensity (I_{inc}) increases slowly from zero, the transmitted intensity (I_{tr}) first increases slowly. If the input reaches the upswitching threshold value (about 6228.3 kW/m^2), I_{tr} jumps into a higher value (from state 1 to 1', see Fig. 11.a). Then I_{tr} increases slowly again as we increase the value of I_{inc}. On the other hand, when I_{inc} is decreased from the value that is greater than the threshold value, I_{tr} decreases slowly from the high value. When I_{inc} reaches the threshold value (state 1'), I_{tr} does not jump back to lower value (state 1), but it remains to decrease slowly until it reaches state 2, at which it jumps to state 2'. Then I_{tr} continues to decrease with decreasing I_{inc}. Thus, the nonlinear defect structure can implement an optical bistability. It should be noticed that the line between the low-output state and high-output state, i.e. the line which connects the state 1 and state 2, corresponds to the unstable solutions.

While the upswitching threshold value for $\omega = 0.995 \times 2\pi c/\lambda_0$ is very large, this value can be reduced by tuning the frequency of the input light closer to the defect mode. For example, the thresholds for $\omega = 0.997 \times 2\pi c/\lambda_0$ and $\omega = 0.999 \times 2\pi c/\lambda_0$ are 1392.8 kW/m^2 and 81.2 kW/m^2 respectively. However, the bistable behavior can not be obtained anymore when the input field has frequency that is very close to the resonance frequency, e.g. in the case of $\omega = 0.9995 \times 2\pi c/\lambda_0$, see Fig. 11.b. We remark that the change of refractive index due to the Kerr nonlinearity that corresponds to the incident intensity 6228.3 kW/m^2 is ~ 0.0412, which is relatively large. When the intensity threshold is reduced to 81.2 kW/m^2, the corresponding refractive index change is ~ 0.0063.

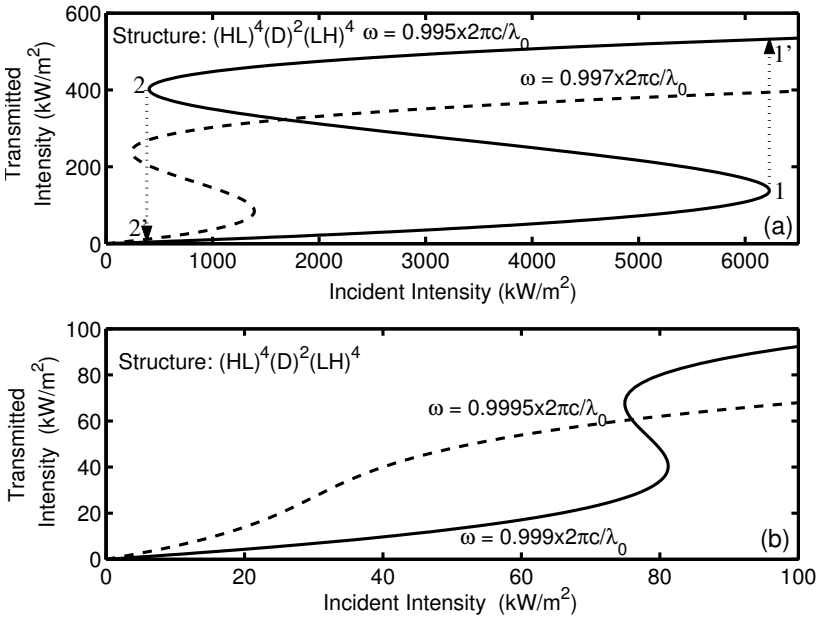

Figure 11: The input-output characteristics of a structure $(HL)^4 (D)^2 (LH)^4$ with $n_d = n_H$ for different frequencies where the Kerr nonlinearity is introduced in all high index layers. The bistability threshold decreases when the input light frequency is closer to the defect mode. However, when the frequency is too close to the defect mode (the case of $\omega = 0.9995 \times 2\pi c/\lambda_0$) the bistability cannot be obtained anymore.

Now we investigate the effect of the defect thickness to the threshold of the bistability. We show in Fig. 12.a the bistability curve of structure $(HL)^4 (D)^M (LH)^4$ for $M = 2, 4, 6$. The optical bistability thresholds are ~ 62.28 kW/m^2 for $M = 4$ and ~ 28.29 kW/m^2 for $M = 6$. It was noticed in the previous section that increasing the defect size does not influence the field enhancement factor but it reduces the FWHM of the defect mode. Therefore we change ω together with M in Fig. 12.a. We conclude that the narrower the width of the defect mode, the lower the threshold of the bistability will be achieved. This qualitative behavior agrees with the result of the FDTD analysis done by Lixue *et al.* [20].

Based on the previous analysis, for a fixed Kerr constant, the bistability threshold is reduced when the width of the defect mode is smaller or when the enhancement factor is larger. Since an increasing number of grating periods produces a smaller FWHM and simultaneously enlarges the enhancement factor, we can expect that a higher number of periods will produce optical bistability with a lower threshold. And indeed, a very low threshold is already obtained when we use a defect structure $(HL)^N (D)^2 (LH)^N$ for $N = 5$ or $N = 6$. The bistability thresholds in these cases are about 7.55 kW/m^2 for $N = 5$ and about 0.96 kW/m^2 for $N = 6$ (see Fig. 12.b). The change of refractive index which corresponds to the latter case is only $\sim 7.6 \times 10^{-4}$.

4 Conclusions

We have presented a new approach to solve the NLH together with the exact transparent (-influx) boundary conditions based on the variational method. In the previous study [16], the nonlinear problem may have non unique solutions and therefore we implement the weighted-averaged fixed point iterative method. The new approach leads to a unique solution and only needs a standard fixed-point iterative method. Therefore it is more robust and more efficient.

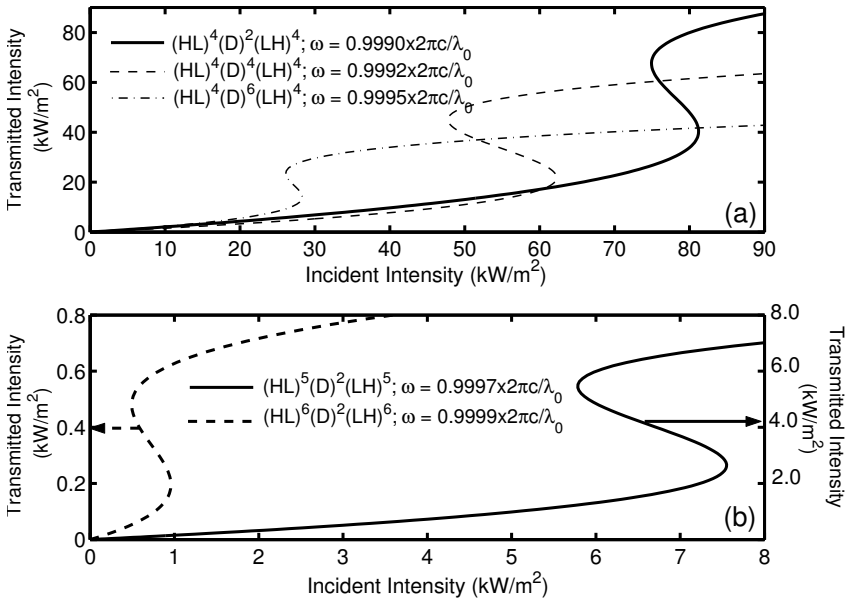

Figure 12: The input-output characteristics of structures $(HL)^N (D)^M (LH)^N$ with $n_d = n_H$ for different M and N where the Kerr nonlinearity is introduced in all high index layers: (a) $N = 4$ and $M = 2, 4, 6$; (b) $M = 2$ and $N = 5, 6$. In (b) the axis on the left hand side is meant for the structure $N = 5$ and $M = 2$, the transmission for structure $N = 6$ and $M = 2$ is to be found on the right hand axis.

The new scheme has been implemented to study the optical response of linear and nonlinear quarter-wavelength reflectors with a defect. It is found that the shape of a defect mode depends on the defect thickness, the position and the refractive index of the defect layer as well as on the number of the grating periods. When the defect thickness is less (greater) than $\lambda_0/4n_d$ then acceptor (donor) modes can be observed in the band gap of the perfect structure. It is found that an optimal field enhancement is obtained when the defect layer is placed in the middle of the structure with the defect thickness being a multiple of $\lambda_0/2n_d$. Increasing the defect thickness yields a smaller spectral width of the defect mode. A larger enhancement factor and simultaneously a narrower FWHM can be achieved by increasing the number of layer periods. When a Kerr medium is present in a defect structure which has good optical features (large field enhancement and narrow resonance) and the frequency of the incident light is selected to be close to the defect mode, optical bistability with a very low threshold can be obtained.

Acknowledgement

This research is supported by the Technology Foundation STW (TWI. 4813), applied science division of NWO and the technology programme of the Ministry of Economic Affairs, The Netherlands. The authors appreciate the valuable discussions with H.J.W.M. Hoekstra and F.P.H. van Beckum.

References

[1] J.D. Joannopoulos, R.D. Meade and J.N. Winn, *Photonic Crystals* (Princeton University Press, Princeton, NJ, 1995).

[2] C.M. Soukoulis (ed.), *Photonic Band Gaps and Localization* (Plenum, New York, 1993).

[3] C.M. Soukoulis (ed.), *Photonic band gap materials* (Kluwer Academic, Dordrecht, 1996).

[4] M. Scalora, J.P. Dowling, C.M. Bowden and M.J. Bloemer, *Phys. Rev. Lett.* **73**, 1369 (1994).

[5] R. Wang, J. Dong and D.Y. Xing, *Phys. Rev.* **E55**, 6301 (1997).

[6] E. Yablonovitch, T.J. Gmitter, R.D. Meade, A.M. Rappe, K.D. Brommer and J.D. Joannopoulos, *Phys. Rev. Lett.* **67**, 3380 (1991).

[7] J.H. Marburger and F.S. Felber, *Phys. Rev.* **A17**, 335 (1978).

[8] H.G. Winful, J.H. Marburger and E. Garmire, *Appl. Phys. Lett.* **35**, 379 (1979).

[9] J. Danckaert, H. Thienpont, I. Veretennicoff, M. Haelterman, and P. Mandel, *Opt. Comm.* **71**, 317 (1989).

[10] J. Danckaert, K. Fobelets, I. Veretennicoff, G. Vitrant and R. Reinisch *Phys. Rev.* **B44**, 8214 (1991).

[11] G.S. Agarwal and S. Dutta Gupta, *Opt. Lett.* **12**, 829 (1987).

[12] S. Dutta Gupta and G.S. Agarwal, *J. Opt. Soc. Am.* **B4**, 691 (1987).

[13] W. Chen and D.L. Mills, *Phys. Rev.* **B35**, 524 (1987).

[14] W. Chen and D.L. Mills, *Phys. Rev.* **B36**, 6269 (1987).

[15] E. Lidorikis, K. Busch, Q.M. Li, C.T. Chan, and C.M. Soukoulis, *Phys. Rev.* **B56**, 15090 (1997).

[16] A. Suryanto, E. van Groesen, M. Hammer and H.J.W.M. Hoekstra, *Opt. Quant. Electr.*, accepted (2002).

[17] R.P. Stanley, R. Houdre, U. Oesterle, M. Ilegems and Weisbuch, Phys. Rev. **A48**, 2246 (1993).

[18] R. Wang, J. Dong and D.Y. Xing, *Phys. Stat. Sol. (b)* **200**, 529 (1997).

[19] G.S. He and S.H. Liu, *Physics of Nonlinear Optics* (World Scientific, Singapore, 1999).

[20] C. Lixue, D. Xiaoxu, D. Weiqiang, C. Liangcai, and L. Shutian, *Opt. Comm.* **209**, 491 (2002).